HHS Public Access

Author manuscript

Eur J Med Genet. Author manuscript; available in PMC 2017 October 01.

Published in final edited form as:

Eur J Med Genet. 2016 October ; 59(10): 540–545. doi:10.1016/j.ejmg.2016.08.012.

Whole Exome Sequencing Identifies a Homozygous *POLG2* Missense Variant in an Infant with Fulminant Hepatic Failure and Mitochondrial DNA Depletion

Hemant Varma[1,5], **Phyllis L. Faust**[1], **Alejandro D. Iglesias**[2], **Stephen M. Lagana**[1], **Karen Wou**[3], **Michio Hirano**[4], **Salvatore DiMauro**[4], **Mahesh M. Mansukani**[1,5], **Kirsten E. Hoff**[6], **Peter L. Nagy**[1,5], **William C. Copeland**[6,*], and **Ali B. Naini**[1,5,*]

[1]Department of Pathology and Cell Biology, Columbia University, 630 W, 168th Street, New York, NY 10032

[2]Division of Medical Genetics, Columbia University, New York Presbyterian Hospital

[3]Division of Genetics, New York Presbyterian Hospital

[4]Department of Neurology, Columbia University Medical Center

[5]Division of Personalized Genomic Medicine, Department of Pathology and Cell Biology, Columbia University Medical Center

[6]Genome Integrity and Structural Biology Laboratory, National Institute of Environmental Health Sciences, NIH, Research Triangle Park, NC 27709

Abstract

Mitochondrial DNA (mtDNA) depletion syndrome manifests as diverse early-onset diseases that affect skeletal muscle, brain and liver function. Mutations in several nuclear DNA-encoded genes cause mtDNA depletion. We report on a patient, a 3-month-old boy who presented with hepatic failure, and was found to have severe mtDNA depletion in liver and muscle. Whole-exome sequencing identified a homozygous missense variant (c.544C>T, p.R182W) in the accessory subunit of mitochondrial DNA polymerase gamma (*POLG2*), which is required for mitochondrial DNA replication. This variant is predicted to disrupt a critical region needed for homodimerization of the POLG2 protein and cause loss of processive DNA synthesis. Both parents were phenotypically normal and heterozygous for this variant. Heterozygous mutations in *POLG2* were previously associated with progressive external ophthalmoplegia and mtDNA deletions. This is the first report of a patient with a homozygous mutation in *POLG2* and with a clinical presentation of severe hepatic failure and mitochondrial depletion.

*Corresponding authors: Ali B. Naini PhD, 630 W 168th Street, P&S 17-401 New York, NY 10032, Phone: (212) 305-1476; Fax: 212-342-0420; abn2@cumc.columbia.edu, William C. Copeland PhD, Genome Integrity and Structural Biology Laboratory, National Institute of Environmental Health Sciences, NIH, Research Triangle Park, NC 27709. Phone: (919) 541-4792; FAX: (919) 541-7613; copelan1@niehs.nih.gov.

DECLARATION OF CONFLICT OF INTEREST.

None.

Keywords

Mitochondrial DNA depletion; *POLG2*; hepatic failure; whole-exome sequencing; *POLG*

INTRODUCTION

Mitochondrial DNA (mtDNA) depletion syndrome (MDS) comprises a genetically and clinically heterogeneous group of autosomal recessive disorders. These disorders are characterized by a profound decrease in mtDNA content that progressively impairs energy production in multiple organ systems [Poulton and Holt 2009]. MDS has three major clinical presentations that include myopathic, encephalomyopathic, and hepatocerebral forms [Finsterer and Ahting 2013]. Onset can be in early infancy or childhood, or less frequently in adulthood [El-Hattab and Scaglia 2013; Suomalainen and Isohanni 2010].

Nuclear DNA-encoded genes maintain the mtDNA copy number, and mutations in several genes lead to mtDNA depletion. These genes are broadly classified into 2 categories: nuclear genes encoding for enzymes involved in mitochondrial nucleotide synthesis (*TK2, SUCLA2, SUCLG1, RRM2B, DGUOK*, and *TYMP*) or those required for mtDNA replication (*POLG* and *C10orf2*) [El-Hattab and Scaglia 2013]. MtDNA replication is accomplished by DNA polymerase gamma, a heterotrimer consisting of one catalytic subunit of DNA polymerase encoded by *POLG* and a dimer of accessory subunits encoded by *POLG2, a* processivity factor for the DNA polymerase [Copeland 2014]. Mutations in *POLG* are a common cause of MDS, and lead to broad and variable phenotypes including progressive external ophthalmoplegia (PEO) with both autosomal dominant and recessive inheritance, myopathy, neurological and hepatocerebral forms [Copeland 2014]. In contrast to *POLG* mutations, only rare cases of heterozygous mutations in *POLG2* causing mtDNA depletion have been described in association with autosomal dominant PEO and muscle weakness (MIM 610131, PEOA4) [Longley and others 2006; Walter and others 2010; Young and others 2011].

Here, we report a 3-month-old boy who presented with fulminant neonatal hepatic failure. We found severe mtDNA depletion in liver and muscle, and partial depletion in blood lymphocytes. Whole-exome sequencing (WES) revealed a homozygous missense variant in *POLG2* that is predicted to be deleterious. There was no history of consanguinity, but both parents were heterozygous for this variant. This patient is the first report of *POLG2* homozygous mutation, with associated mtDNA depletion and hepatic failure in infancy.

CLINICAL DESCRIPTION

The infant was a male born at 37 weeks via cesarean section, after an uncomplicated pregnancy with a birth weight of 3.5 kg. Parents were healthy: both father (age 43) and mother (age 36 year) were from the same town but non-consanguineous. The patient has a healthy 5-year-old brother. The mother had 2 early first trimester miscarriages (6 and 8 weeks), and a stillbirth at 8 months from likely placental insufficiency based on autopsy. Family history in parent’s siblings, sibling’s children, and grandparents was negative for liver disease, metabolic disorders, ophthalmoplegia, or any other major illness. He was discharged without complications. The infant was healthy until 3 months of age when he

presented to another institution with a one-week history of decreased oral intake, difficult breathing, and abdominal distention. On admission he was found to have profound metabolic acidosis with an anion gap of 21 mEq/L (normal 3–11 mEq/L), moderate hyperkalemia, and increased lactate 14 mmol/L (normal 0.5–1.6 mmol/L). Coagulopathy with elevated INR of 3.0 (normal 0.9–1.2) was noted in the setting of elevated liver enzymes (AST 244 U/L, normal 12–38 U/L and ALT 151 U/L, normal 7–41 U/L), elevated total bilirubin level of 8.0 mg/dL (normal 0.3–1.3 mg/dL) with direct bilirubin of 4.6 mg/dL (normal, 0–0.4 mg/dL), elevated bile acids at 229 μmol/L (normal 1–10 μmol/L), normal GGT and decreased albumin 2.8 g/dL (normal, 3.5–5.5 g/dL). He was transferred to our institution for fulminant hepatic failure after intubation for impending respiratory failure. He was subsequently stabilized, metabolically compensated and extubated. At initial consultation, the infant was breathing spontaneously and was alert. He had mild jaundice. Other than an upturned nose and low nasal bridge, there were no dysmorphic features. The abdomen was distended with a firm liver edge felt 1–2 cm below the rib cage; the spleen was not palpable. Subsequent neurological examination was unremarkable with normal muscle tone. Brain MRI showed thinning of the corpus callosum. Myelination pattern was within normal limits for the patient's age. There were subtle diffusion abnormalities involving bilateral hippocampal formations but no evidence of abnormal enhancement or signal abnormalities to suggest an infectious or inflammatory process. In addition, MR spectroscopy demonstrated small lactate peaks in the left basal ganglia and left frontal white matter.

METHODS

Histo-chemical studies

Analysis of muscle using 8-micrometer-thick sections were carried out as previously described [Tanji and Bonilla 2001].

Electron microscopy

An ultra-thin section of liver was examined with a JEOL 1011 electron microscope (JEOL, Tokyo, Japan) using magnifications that ranged from 5,000 to 60,000×.

Mitochondrial DNA copy number determination

Multiplex Real-time PCR was employed to determine the copy number of mitochondrial DNA in blood leukocytes, muscle, and liver tissues using a TaqMan assay as previously described [Cossarizza and others 2003] with minor modifications. Briefly, short segments of the ND2 gene in mtDNA and the FASLG gene in nuclear DNA (nDNA) were simultaneously amplified in the presence of fluorescently labeled probes. All amplifications were carried out on a 7500 Fast Real-Time PCR System (Applied Biosystems, USA) and data analyses were performed using 7500 V.O.6 software. To ensure an accurate determination of mtDNA and nDNA copy number, different concentrations of a single reference plasmid that contained one copy of each of the appropriate regions of mtDNA and nDNA were included in the assay, and copy numbers were calculated from the standard curve. The control DNA was from 2 females, aged 14 and 16 years and 1 male, age 6 years, these controls did not have any evidence of mitochondrial DNA depletion syndrome.

Whole-exome sequencing (WES)

WES was performed on whole genome-amplified DNA obtained from the blood of the patient using Illumina Hiseq2500. Hybrid capture method was used to isolate 70 megabases of targeted DNA that included the 16 kb mtDNA and all coding and untranslated exons of 1423 nuclear genes, including 1013 mitochondrial genes from the MitoCarta databases [Pagliarini and others 2008]. De novo, homozygous or compound heterozygous variants with allele frequencies of less than 1% in the general population were further analyzed. Clinically significant variants were confirmed using Sanger sequencing of the proband and both parents.

Molecular modeling

The human apo POLG2 structure (PDB: 2G4C) [Fan and others 2006] was examined using PyMol (The PyMOL Molecular Graphics System, Version 1.7.4 Schrödinger, LLC). The mutagenesis wizard was utilized to mutate R182 to W and the rotamer with the fewest clashes was chosen.

RESULTS

Mitochondrial and other metabolic disorders were in the differential diagnosis based on the clinical presentation and initial laboratory findings. Further work-up included infectious screen, complete metabolic panel, liver and muscle biopsies, mitochondrial DNA studies on peripheral blood, muscle and liver tissue, and WES. An infectious etiology for the liver failure was ruled out by testing for Adenovirus, Parvovirus, CMV, EBV, RPR, HSV 1 + 2, Hepatitis A, Hepatitis B, Hepatitis C and HIV 1 + 2. Extensive metabolic work-up was conducted. Ammonia was normal but pyruvate was elevated at 0.23 mM/L (normal 0.04–0.13 mM/L). Although the total and free carnitine levels were normal, elevations of many long chain and long chain 3-hydroxyacylcarnitine were consistent with mitochondrial dysfunction. Plasma amino acid analysis showed increased levels of methionine at 558 μM (normal 10–60 μM) and tyrosine at 328 μM (normal 30–140 μM) in the absence of plasma succinylacetone, consistent with significant hepatic dysfunction. Also, urinary organic acid analysis showed increased levels of lactate and pyruvate, likely secondary to impaired mitochondrial function. Presence of normal levels of plasma very long chain fatty acids reduced the likelihood of many peroxisomal disorders and the absence of urinary reducing substances also reduced the likelihood of some disorders of simple carbohydrate metabolism such as galactosemia. Liver biopsy performed at 3 months of age showed microvesicular steatosis with cholestasis and abundant pan-lobular fibrosis (Fig. 1A). Electron microscopic examination of liver tissue highlighted profound microvesicular steatosis (multiple vacuoles) and mild to moderate pleomorphism in size and shape of mitochondria, including hyperplastic forms, abnormal curvilinear and circular cristae morphology and filling of the mitochondrial matrix with granular material (Fig. 1 B and C). These findings suggested a mitochondrial disorder. Muscle biopsy showed no diagnostic abnormalities in hematoxylin-eosin stain (Fig. 1D). Enzyme histochemistry for cytochrome oxidase (COX) and combined COX and succinate dehydrogenase (SDH) did not reveal any significant deficiency in COX staining and no ragged-blue fibers (COX-negative, SDH-positive) were seen (Fig. 1 E, F). Electron microscopy of muscle showed mild ultrastructural alterations in mitochondria

similar to those seen in the liver (data not shown); no paracrystalline mitochondrial inclusions were evident in either liver or muscle.

The copy number of mtDNA were determined by Multiplex real-time PCR with the mtDNA levels normalized to the nuclear DNA gene (see Methods). Severe mtDNA depletion was seen in the liver (25% of control) and muscle (20%), and partial depletion in blood leukocytes (44%) (Fig. 2A). However, there was no evidence of any mtDNA deletions or rearrangements as assessed by Southern blot of blood leukocyte, muscle and liver DNA. Furthermore, sequencing of the mitochondrial genome from blood leukocytes was negative for known pathogenic point mutations.

WES was performed on DNA derived from the patient's peripheral blood using Illumina Next-Generation sequencing and our in-house analysis pipeline (see Methods). We identified two homozygous missense variants, one each in *POLG2* and *SOX17*, and a homozygous intronic variant in the *INTS2* gene (c.456+5A>G) that is +5 from the intron-exon 3 boundary and is not expected to affect the canonical splicing sites. *INTS2* (OMIM 611346) is not associated with any disease. The variant information and quality metrics are provided in Tables 1 and 2. Mutations in the *SOX17* are associated with autosomal dominant genitourinary tract malformations (MIM 613674), indicating that the variants in *SOX17* and *INTS2* were unlikely to explain the patient's phenotype. We identified a homozygous missense variant in *POLG2* (Chr17: 62492543G>A, NM_007215.3, NP_009146.2 c. 544C>T, p.Arg182Trp (pR182W)) (Fig. 3A). Sanger sequencing confirmed this homozygous variant in the patient (Fig. 3B) and revealed that both parents were heterozygous for this variant. This variant is not previously reported in publicly available databases including ExAC, EVS and 1000 genomes. *In silico* analysis predicted that this variant had a deleterious (Provean −6.39) and damaging (PolyPhen-2 and SIFT (0.000)) effect on the protein's function. Arg182 is at the base of the four-helix bundle that is critical to dimerization [Carrodeguas and others 2001] (Fig. 4A). The substitution of arginine with tryptophan at residue 182 in the POLG2 protein subunit is predicted to disrupt essential H-bonds between the $\mathbf{N_{\delta}}$ nitrogen and the carboxy backbone at Val213, the $\mathbf{N_{\omega}}$ nitrogen to the carboxy backbones of Ala130 and Leu131, as well as an H-bond to the side chain of His132 (Fig. 4 B, C). Also the substitution of tryptophan at position 182 causes a steric clash between the N1 of Trp182 and the carboxy of Val213 (Fig. 4C, red arc). The Arg182 residue in POLG2 is conserved across vertebrates (Fig. 4D), where it exists as a dimer [Young and Copeland 2013], but is not conserved in insects, in which POLG2 exist as monomers. Thus the Arg182Trp substitution may disrupt POLG2 dimerization.

DISCUSSION

MDS are a group of early-onset recessively inherited disorders that can be caused by mutations in one of at least nine nuclear genes [El-Hattab and Scaglia 2013; Suomalainen and Isohanni 2010]. Mutations in *POLG, DGUOK, MPV17*, and *TWINKLE* are the common causes of infantile hepatocerebral form of the disease, whereas those in *TK2* and *SUCLA2* cause severe myopathic form of the disease [El-Hattab and Scaglia 2013]. In our patient, we excluded other genetic causes of mtDNA depletion (mutations in *TK2, DGOUK, MPV17, SUCLA2, SUCLG1* and *RRM2B*). MDS can present with hepatic failure in

infancy. A report of 10 infants presenting with severe hepatic failure and mitochondrial depletion showed several ultrastructural abnormalities including microvesicular steatosis and altered mitochondrial morphology, features similar to those observed in this patient [Mandel and others 2001]. Notably, homozygous deletion of *Polg2* in mice causes embryonic lethality. Electron microscopic analysis of *Polg2* (−/−) in mouse embryos showed severe ultra-structural defects with loss of organized cristae in mitochondria, and increased lipid accumulation [Humble and others 2013], similar to the abnormalities observed in this patient (Fig. 1). However, we did not see ragged-blue fibers, a classic hallmark of mitochondrial myopathies that result from accumulation of defective mitochondria, though these changes are not always present in neonatal-infantile mitochondrial muscle disease. [Bourgeois and Tarnopolsky 2004]. Nearly 250 pathogenic *POLG* mutations have been reported [Copeland 2014] and these are associated with clinical phenotypes ranging from mild adult-onset CPEO to rapidly fatal Alpers-Huttenlocher syndrome characterized by myopathy, hepatopathy and intractable seizures. In contrast to *POLG*, to date, only two heterozygous mutations of *POLG2* have been described, and these are associated with late-onset autosomal dominant PEO with multiple mtDNA deletions (OMIM 610131) [Longley and others 2006; Walter and others 2010; Young and others 2011]. *POLG2* encodes the accessory subunit of DNA polymerase γ, and is required for imparting high processivity to POLG by increasing the affinity of the protein complex to DNA [Lim and others 1999]. Biochemical and functional studies of one pathogenic missense mutation (c.1352G>A; p.G451E) showed decreased processivity of the enzyme complex leading to multiple mitochondrial DNA deletions [Young and others 2015; Young and others 2011]. The second reported heterozygous insertion (c.1207–1208ins24) mutation causes mis-splicing and skipping of exon 7, thereby impairing the C-terminal domain that is required for processivity [Walter and others 2010].

The p.Arg182Trp mutation in POLG2 described here, is the first reported homozygous mutation in this gene. The fact that both apparently healthy parents (obligate carriers) were heterozygous for the variant suggests that this mutation either has an autosomal recessive pattern of inheritance, or that PEO has a late onset, and is yet to manifest in the apparently normal parents. Molecular modeling and evolutionary comparisons suggest that the R182W substitution may impact the dimerization of POLG2 (Fig. 4) [Oliveira and others 2015] [Yakubovskaya and others 2006].

In summary, this is the first report of a patient with a homozygous loss of function of *POLG2* associated with neonatal fulminant liver failure due to severe mtDNA depletion. This report adds *POLG2* to the list of genes causing mtDNA depletion syndrome with hepatic insufficiency presenting in infancy.

Acknowledgments

Part of this research was supported by National Institutes of Health grants 5P01 HD080642-02 NIH/NICHD (to ABN) and the Intramural Research Program of the NIH, National Institute of Environmental Health Sciences (ES 065078 to WCC). We thank the CUMC Neuromuscular Laboratory for performing the enzyme histochemistry staining of the muscle biopsy. The variant has been submitted to the ClinVar database (**Submission number: SUB1740227**).

REFERENCES

Bourgeois JM, Tarnopolsky MA. Pathology of skeletal muscle in mitochondrial disorders. Mitochondrion. 2004; 4(5–6):441–452. [PubMed: 16120405]

Carrodeguas JA, Theis K, Bogenhagen DF, Kisker C. Crystal structure and deletion analysis show that the accessory subunit of mammalian DNA polymerase gamma, Pol gamma B, functions as a homodimer. Mol Cell. 2001; 7(1):43–54. [PubMed: 11172710]

Copeland WC. Defects of mitochondrial DNA replication. J Child Neurol. 2014; 29(9):1216–1224. [PubMed: 24985751]

Cossarizza A, Riva A, Pinti M, Ammannato S, Fedeli P, Mussini C, Esposito R, Galli M. Increased mitochondrial DNA content in peripheral blood lymphocytes from HIV-infected patients with lipodystrophy. Antivir Ther. 2003; 8(4):315–321. [PubMed: 14518701]

El-Hattab AW, Scaglia F. Mitochondrial DNA depletion syndromes: review and updates of genetic basis, manifestations, and therapeutic options. Neurotherapeutics. 2013; 10(2):186–198. [PubMed: 23385875]

Fan L, Kim S, Farr CL, Schaefer KT, Randolph KM, Tainer JA, Kaguni LS. A novel processive mechanism for DNA synthesis revealed by structure, modeling and mutagenesis of the accessory subunit of human mitochondrial DNA polymerase. J Mol Biol. 2006; 358(5):1229–1243. [PubMed: 16574152]

Finsterer J, Ahting U. Mitochondrial depletion syndromes in children and adults. Can J Neurol Sci. 2013; 40(5):635–644. [PubMed: 23968935]

Humble MM, Young MJ, Foley JF, Pandiri AR, Travlos GS, Copeland WC. Polg2 is essential for mammalian embryogenesis and is required for mtDNA maintenance. Hum Mol Genet. 2013; 22(5): 1017–1025. [PubMed: 23197651]

Lim SE, Longley MJ, Copeland WC. The mitochondrial p55 accessory subunit of human DNA polymerase gamma enhances DNA binding, promotes processive DNA synthesis, and confers N-ethylmaleimide resistance. J Biol Chem. 1999; 274(53):38197–38203. [PubMed: 10608893]

Longley MJ, Clark S, Yu Wai Man C, Hudson G, Durham SE, Taylor RW, Nightingale S, Turnbull DM, Copeland WC, Chinnery PF. Mutant POLG2 disrupts DNA polymerase gamma subunits and causes progressive external ophthalmoplegia. Am J Hum Genet. 2006; 78(6):1026–1034. [PubMed: 16685652]

Mandel H, Hartman C, Berkowitz D, Elpeleg ON, Manov I, Iancu TC. The hepatic mitochondrial DNA depletion syndrome: ultrastructural changes in liver biopsies. Hepatology. 2001; 34(4 Pt 1): 776–784. [PubMed: 11584375]

Oliveira MT, Haukka J, Kaguni LS. Evolution of the metazoan mitochondrial replicase. Genome Biol Evol. 2015; 7(4):943–959. [PubMed: 25740821]

Pagliarini DJ, Calvo SE, Chang B, Sheth SA, Vafai SB, Ong SE, Walford GA, Sugiana C, Boneh A, Chen WK, Hill DE, Vidal M, Evans JG, Thorburn DR, Carr SA, Mootha VK. A mitochondrial protein compendium elucidates complex I disease biology. Cell. 2008; 134(1):112–123. [PubMed: 18614015]

Poulton J, Holt IJ. 163rd ENMC International Workshop: nucleoid and nucleotide biology in syndromes of mitochondrial DNA depletion myopathy 12–14 December 2008, Naarden, The Netherlands. Neuromuscul Disord. 2009; 19(6):439–443. [PubMed: 19464176]

Suomalainen A, Isohanni P. Mitochondrial DNA depletion syndromes--many genes, common mechanisms. Neuromuscul Disord. 2010; 20(7):429–437. [PubMed: 20444604]

Tanji K, Bonilla E. Optical imaging techniques (histochemical, immunohistochemical, and in situ hybridization staining methods) to visualize mitochondria. Methods Cell Biol. 2001; 65:311–332. [PubMed: 11381601]

Walter MC, Czermin B, Muller-Ziermann S, Bulst S, Stewart JD, Hudson G, Schneiderat P, Abicht A, Holinski-Feder E, Lochmuller H, Chinnery PF, Klopstock T, Horvath R. Late-onset ptosis and myopathy in a patient with a heterozygous insertion in POLG2. J Neurol. 2010; 257(9):1517–1523. [PubMed: 20405137]

Yakubovskaya E, Chen Z, Carrodeguas JA, Kisker C, Bogenhagen DF. Functional human mitochondrial DNA polymerase gamma forms a heterotrimer. J Biol Chem. 2006; 281(1):374–382. [PubMed: 16263719]

Young, MJ.; Copeland, WC. Mitochondrial disorders associated with the mitochondrial DNA polymerase γ: A focus on intersubunit interactions. In: Wong, LJC., editor. Mitochondrial disorders caused by nuclear genes, 1e. New York: Springer; 2013. p. 49-72.

Young MJ, Humble MM, DeBalsi KL, Sun KY, Copeland WC. POLG2 disease variants: analyses reveal a dominant negative heterodimer, altered mitochondrial localization and impaired respiratory capacity. Hum Mol Genet. 2015; 24(18):5184–5197. [PubMed: 26123486]

Young MJ, Longley MJ, Li FY, Kasiviswanathan R, Wong LJ, Copeland WC. Biochemical analysis of human POLG2 variants associated with mitochondrial disease. Hum Mol Genet. 2011; 20(15): 3052–3066. [PubMed: 21555342]

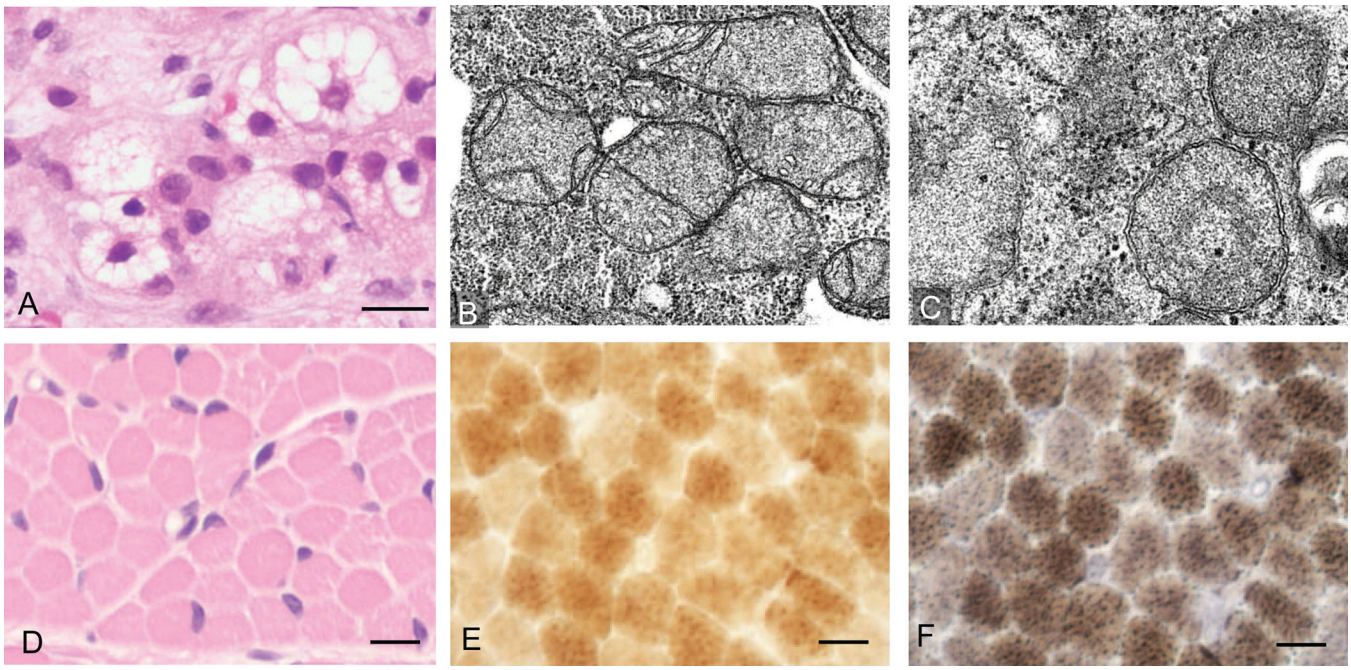

Figure 1.

Histological and ultrastructural evidence for hepatic microsteatosis and mitochondrial structural defects. (A) Hematoxylin and eosin-stained sections of liver biopsy show microsteatosis (multiple vacuoles) in the cytoplasm (scale bar 10μm). (B–C) Electron microscopic examination of liver shows structural abnormalities in mitochondria (B) 20,000× and (C) 30,000×. (D) Muscle biopsy of right quadriceps muscle stained with hematoxylin and eosin (scale bar 20μm). (E–F) Staining for (E) COX and (F) combined SDH and COX, these stains showed no evidence of COX deficient fibers or ragged-blue fibers (scale bar 10μm).

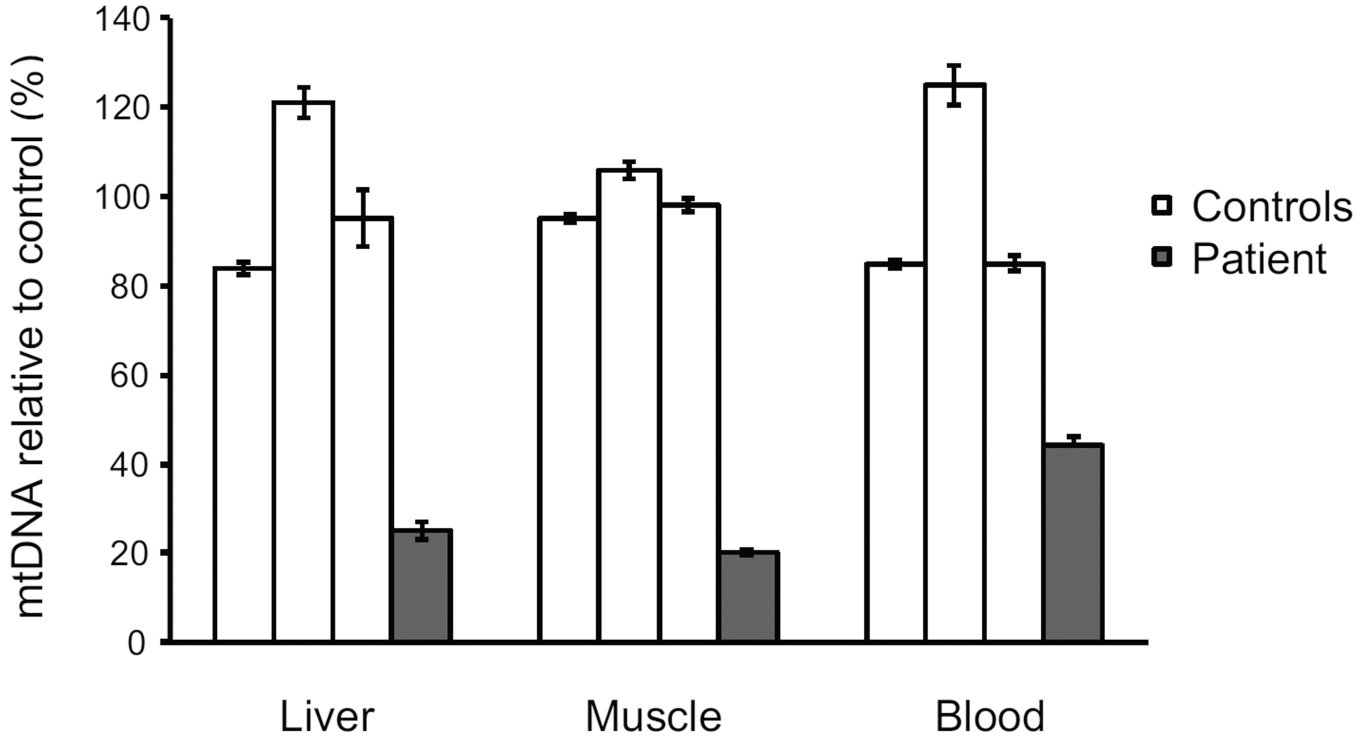

Figure 2.

Mitochondrial DNA depletion in various tissues. Mitochondrial DNA levels were measured by Multiplex Real-time PCR in liver and muscle (frozen tissue) and blood lymphocytes. The mean mtDNA levels of the 3 control samples was set as 100%. The relative mtDNA levels are expressed as mean +/− SEM for each control and patient sample, each sample was tested in triplicate.

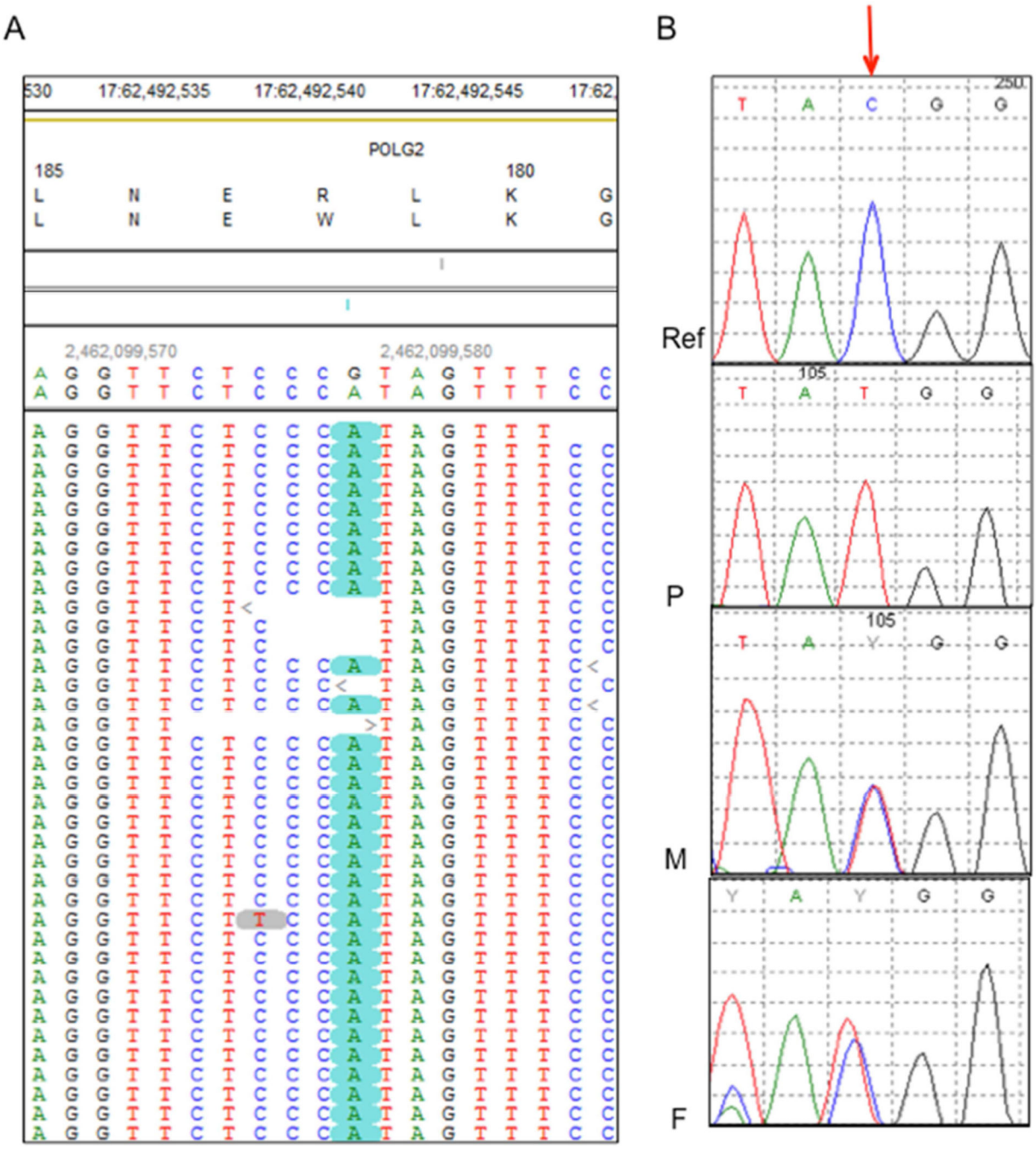

Figure 3.

Sequencing shows a *POLG2* homozygous missense variant. (A) Pile-up of the reads from Next-Gen sequencing shows the homozygous c.544C>T (G>A in the genomic complementary sequence), p.R182W variant. The variant is highlighted in green. (B) Sanger sequencing of variant (Reference sequence (Ref), patient (P), mother (M) and father (F)). The red arrow points to the nucleotide with the homozygous (C>T) substitution in the patient and heterozygous variant in both parents.

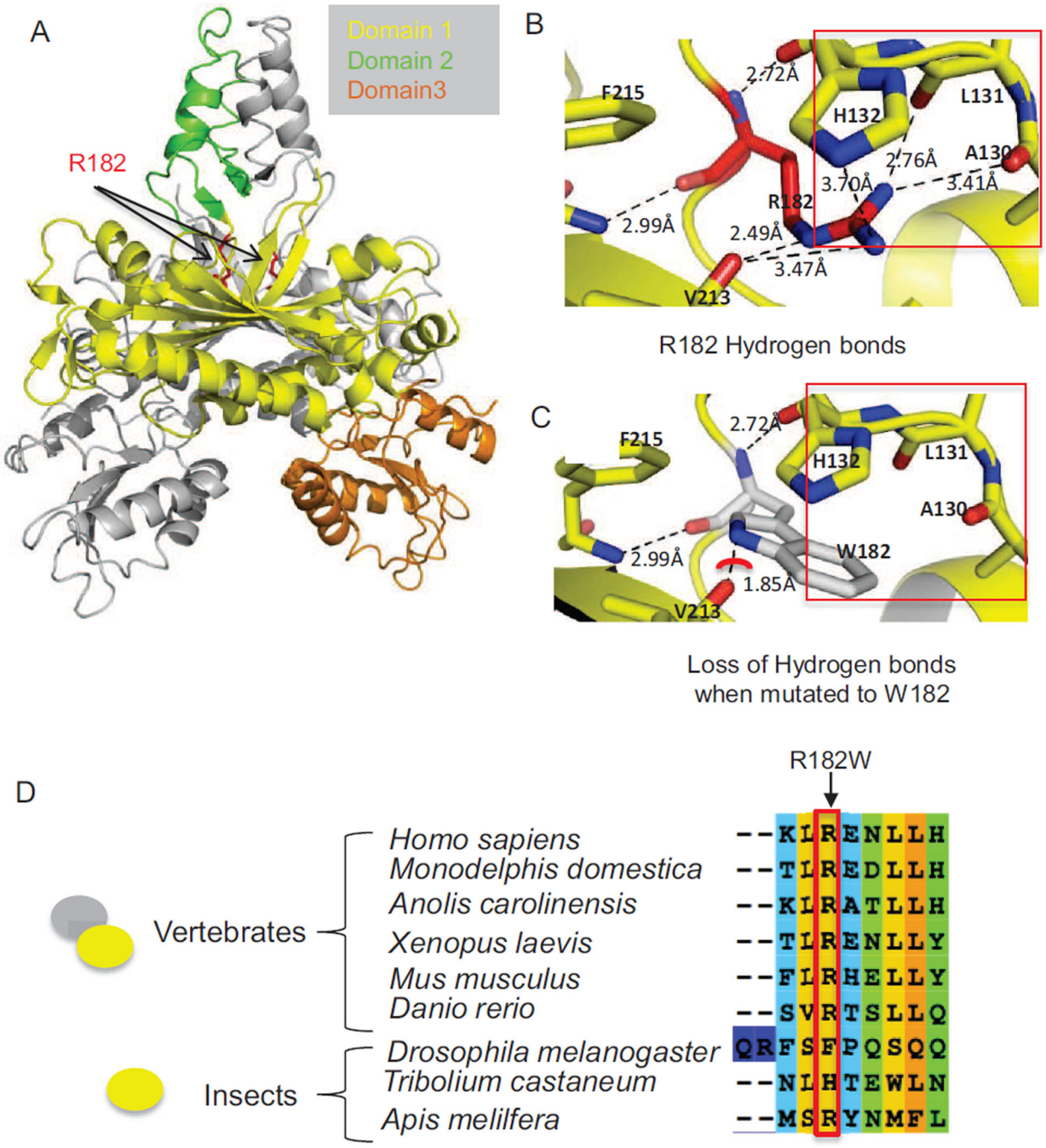

Figure 4.

Structural implications of the R182W mutation in the protein structure of human Pol γ accessory subunit, *POLG2* (PDB: 2G4C) and conservation of R182 in vertebrate POLG2 sequences. (A) Overview of the *POLG2* homodimer illustrating the location of R182. In gray is one monomer of *POLG2* while the other monomer is broken down into domains, with domain 1 in yellow, domain 2 in green and domain 3 in orange. The arrows are pointing to Arg182, which is highlighted in red. (B) Hydrogen bonding interactions of the Arg182 side chain with the carboxy backbone of residues Val213, Leu131, and Ala130, as well as

the side chain of His132, all except V213 are highlighted by the red box. (C) Loss of H-bonding when Arg182 is altered to Trp is highlighted by the red box. The red arc shows a potential steric clash between Arg182 and Val213. (D) The red-box and arrow both highlight Arg182. The oval shapes on the left indicate the oligomerization state of *POLG2*, which exists as a homodimer in vertebrates and a monomer in insects.

Table 1

List of all rare homozygous variants in the proband

Chromosome	**Chr17**	**Chr 8**	**Chr17**
Position	62492543	55370796	60002317
Gene name	*POLG2*	*SOX17*	*INTS2*
Refseq	NM_007215.3	NM_022454.3	NM_020748.2
Reference sequence	G	C	T
PROBAND: number of reads with reference	0	0	2
PROBAND : alternative	A	A	A
PROBAND: number of reads with alternative	212	45	113
Other relative tested (NGS or Sanger) with the result	Father : heterozygous (Sanger) Mother : heterozygous (Sanger)	Unknown	Unknown
Mutation type	Missense	Missense	Intronic
Mutation : DNA (HGVS nomenclature)	c.544C>T	c.98C>A	c.456+5A>G
Mutation : protein (HGVS nomenclature)	p.Arg182Trp	p.Ala33Asp	NA
Prediction < SIFT	Damaging	Damaging	NA
Prediction < PolyPhen-2	Probably damaging	Benign	NA
Prediction < Provean	Deleterious	Deleterious	NA

Table 2

Quality metrics for Next Generation sequencing of Proband

	Proband	**Add other family members (parents, sibs…) as appropriate**
Total captured regions size	70 Mb	NA
% of captured regions with coverage >10	97%	NA
Average coverage of captured region (%)	83 ×	NA
Total number of SNPs	21,680	NA
Total number of INDELs	676	NA
Total number of rare homozygous variants (<1% population frequency)	3	NA